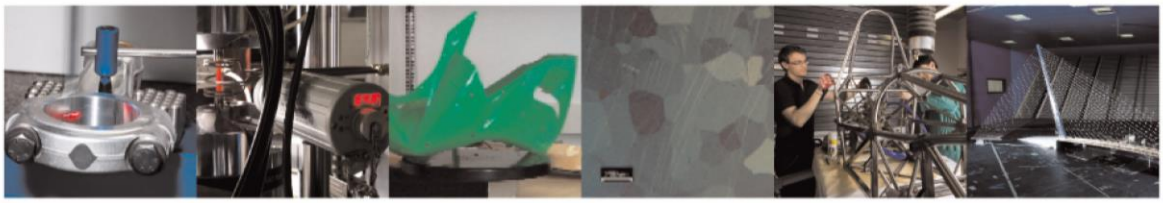

Laser surface texturing of SS316L for enhanced adhesion of HUVECs

Agung, Purnama; Furlan, Valentina; Dessi, D; Demir, Ali Gökhan; Tolouei, Ranna; Paternoster, Carlo; Levesque, Lucie; Previtali, Barbara; Mantovani, Diego

This is an Accepted Manuscript of an article published by Taylor & Francis in Surface Engineering on 12 Jul 2018, available online: https://doi.org/10.1080/02670844.2018.1495408.

Laser surface texturing of SS316L for enhanced adhesion of HUVECs

Agung Purnama[1], Valentina Furlan[1], Desirèe Dessi[1,2], Ali Gökhan Demir[1*], Ranna Tolouei[2], Carlo Paternoster[2], Lucie Levesque[2], Barbara Previtali[1], Diego Mantovani[2]

[1]*Department of Mechanical Engineering, Politecnico di Milano, Via La Masa 1, 20156, Milan, Italy.*

[2]*Laboratory for Biomaterials and Bioengineering (LBB). Canada Research Chair Tier I in Biomaterials and Bioengineering for the Innovation in Surgery, Department of Mining, Metallurgy, and Materials Engineering, Laval University, Quebec City, G1V 0A6, Canada.*

***Corresponding author:**
Dr. Ali Gökhan Demir
Tel: +39 02 2399 8590
Fax: +39 02 2399 8585
Email: aligokhan.demir@polimi.it

Laser surface texturing of SS316L for enhanced adhesion of HUVECs

Abstract

This study investigates the effect of the structured surface to the adhesion, proliferation, and alignment of endothelial cells (HUVECs). The chemical state of laser structured surface was also investigated in comparison with non-treated surface. A novel design for biomedical applications consisting of parallel chain-like structures was realised on stainless steel surface by laser micromachining. The structures were designed to employ surface topography in the presence of micron and sub-micron features and to avoid intensive surface modification that could compromise the mechanical properties of thin devices like cardiovascular stents. The results showed that the structured surfaces favor the adhesion, proliferation, and alignment of HUVECs. The proliferation and the alignment of HUVECs were pronounced when periodic distance between two consecutive chain-like structures was 25 μm. Moreover, there was no significant difference of chemical composition on the structured surface suggesting that the cell proliferation and alignment were mainly influenced by the surface topography.

Keywords: Laser surface texturing; endothelial cells; cardiovascular stents; stainless steel AISI 316L; XPS

1. Introduction

Endothelialisation, or a lack thereof, plays a critical role in the occurrence of thrombosis following the implantation of blood contact devices such as heart valves, catheters, and cardiovascular stents [1]. In a confluent state, the endothelial cell layer produces nitric oxide (NO) contributing to the inhibition of platelet and maintaining the smooth muscle cells (SMC) in a non-proliferative state [2]. The deployment of a cardiovascular stent involves the disruption of the endothelial layer along the artery due to the catheterization, particularly within the atherosclerotic lesion where the balloon is deployed to force the stent against the arterial wall. For this reason, stent deployment is associated to 30-40% smooth muscle over-proliferation or intimal hyperplasia (IH) [3]. Although IH is successfully overcome by the incorporation of anti-proliferative drugs, its long-term occurrence is unavoidable once the drugs are fully eluted [4]. To this end, surface structuring by laser was proposed as a potential option to restore the pivotal layer of endothelial cells.

Laser surface structuring stands out as a promising option being highly precise and flexible in terms of generating different possibilities to enhance surface morphology and chemistry. The use of different wavelengths (ultraviolet to near infrared) and pulse durations (femtosecond to nanosecond) allow for structuring different types of material [5-7]. The process can be used to modify the surface topography both towards flatter [8] and ordered structures [9-11]. Laser structured surfaces are most commonly studied for orthopaedic and dental implants to promote osteointegration [12-15]. Periodic surface microstructures such as grooves [5,16], dimples [12], squares and triangles [17], as well as random textures, have been proposed [18]. Cell adhesion and proliferation are commonly achieved by all surface types of structures, such as pits and posts, which have been explored on stainless steel surface and various polymers. They have been reported to increase the adhesion, density, monolayer formation, and proliferation of endothelial cells [6,7]. Of all the mentioned structures, grooving appears to be the most effective one, as it promotes endothelial cells alignment in addition to any mentioned benefit of the surface structuring [5,17]. However, a grooving dimension as deep as 5 µm could compromise the mechanical properties of thin structure devices such as cardiovascular stents. In fact, this surface feature could constitute a concern, as newer generation of cardiovascular stent bears thinner struts than those of the older ones [19,20]. Therefore, a

surface structure appropriately studied for thin structure medical devices, such as cardiovascular stent applications, is desirable.

The current study was aimed at proposing a novel structure that could promote the adhesion, proliferation, and alignment of endothelial cells. Chemical and physical characterisations of the novel structure were investigated in relation to the behaviour of endothelial cells. To this end, a parallel chain-like structure was proposed and printed on stainless steel surface by laser micromachining (1) to introduce surface topography in the presence of micron and sub-micron features; (2) to avoid intensive surface modification, such as a grooving that could compromise the mechanical properties of thin structured devices like cardiovascular stent. The surface structure was realized by partial melting and ablation through nanosecond-pulsed fiber laser on stainless steel AISI 316L (SS316L). Similar surface structures have been reported in literature for different applications. In this work, their use for manipulating the cell adhesion and proliferation behaviour has been studied by adjusting their spatial distribution. The structure was applied along linear scans over the sample surface. The resulting surface was then analyzed for its chemical composition by XPS analysis. Cellular viability, proliferation, and alignment of endothelial cells were then assessed comparing laser structured surface and as electropolished surface. Different periodic distances between the adjacent chain-like structures were applied to verify if the density of the chain-like structure give influences to the behaviour of endothelial cells.

2. Materials and method

2.1. Laser treatment

SS316L samples (Goodfellow Corporation, PA, USA) with a thickness of 0.2 mm were cut in square sheets measuring 10 mm x 10 mm. Prior to the laser treatment, all the samples were mechanically polished using SiC abrasive paper (from 800 to 1200 grit) then finished with colloidal silica 50 nm. The samples were then washed with acetone, deionized water, and ethanol in ultrasonic bath for 15 minutes each and air dried. Samples were then electropolished and acid dipped as previously described elsewhere[21]. Electropolishing solution for SS316L consists of glycerol 99% (50% v/v), phosphoric acid 85% (35% v/v), and deionized H_2O (15% v/v). The electrolyte was kept at 90°C during the procedure, which was performed at a constant voltage of 60 V; the cathode was made of the same material as the anode. The electropolished samples were then acid dipped in a mixture of nitric acid 70% (10% v/v), hydrofluoric acid 50% (2% v/v), and deionized H_2O (88% v/v). The samples were then rinsed following the previous washing method.

Laser structuring was performed with a pulsed fiber laser operating with 250 ns pulse width and emitting at 1064 nm wavelength (YLP-1/100/50/50 from IPG Photonics, Oxford, MA, USA). The laser source provided a collimated beam at the output, which was focused with processing head housing at 50 mm focal lens (µ from HighYAG, Kleinmachnow, Germany). Sample positioning was achieved via linear axes (ALS-130 from Aerotech, Inc, Pittsburgh, USA). In this configuration the beam diameter on focal plane was determined to be 19.5 µm. Initially the effect of main laser parameters on the micromachined track geometry was studied. Laser pulse energy (E) was varied between 30 and 50 µJ in order to obtain limited machining depth (h) and width (w). Scan speed (v) was varied between 39 and 97 mm/s thus overlapping more or less pulses per area. Pulse repetition rate (PRR) was fixed at 20 kHz. Depth (h) and width (w) of the laser micromachined structures were measured with focus variation microscopy (InfiniteFocus from Alicona Imaging GmbH, Graz, Austria). All samples were laser treated in ambient atmosphere. Table 1 summarizes the details of the experimental plan.

In the second stage, samples were prepared with selected laser parameter combinations as illustrated in Figure 1 (A). The periodic distance (*d*) between the scan lines was varied with regards to the average size of endothelial cells (25 µm). Therefore, the *d* was varied to 25 µm, 75 µm, and 150 µm, suggesting different density of structures on the surfaces. The resulting samples were conventionally labelled as *d*25, *d*75, and *d*150 respectively. They were observed using Scanning Electron Microscope (JSM-840A from Joel Ltd., Tokyo, Japan) in backscattered electron mode with a tungsten filament primary beam emitter at an acceleration voltage of 15 kV. Moreover, surface topography was quantitatively characterized using Atomic Force Microscope (Veeco Instrument Inc., Woodbury, USA) equipped with a silicon probe (tip radius of 2 nm) and assisted by the built-in software Nanoscope Analysis V1.40r1 (Veeco Instrument Inc., Woodbury, USA).

2.2. Characterization of surface chemistry

X-ray photoelectron spectroscopy (XPS) was used to analyse the surface chemical composition of the electrochemically polished and laser structured SS316L. The analysis required an extended width of laser surface structured region due to the sampling spot of the XPS equipment of about 125 µm. For this, a laser structured zone consisting of highly dense chain-liked structured was created to conduct a selective analysis of the laser irradiated area. Prior to XPS analysis, the samples were cleaned in ultrasonic bath for 15 minutes repeatedly with acetone, deionized H_2O, and 70% ethanol. XPS was carried out on a PHI 5600 ESCA System (Physical Electronics USA, MN, USA) instrument using standard Al Kα radiation for survey scan (Kα=1486.6 eV) and Mg Kα for high resolution scan (Kα=1253.6 eV). The survey scans were acquired with a pass energy of 80 eV. The angle between X-ray beam and the analyzer plan was 45_o and photo-electrons were collected normal to the sample surface. Data processing was analyzed using a MatLab-based program with specific macros called Multipak V9.6.0 (Ulvac-Phi Inc., Kanagawa, Japan). The curve fitting for high resolution peaks were determined by means of the least-squares method using Gauss-Lorentz functions with a Shirley background subtraction.

2.3. HUVECs adhesion and proliferation

The primary human vascular endothelial cells (HUVECs) were isolated following the procedure described elsewhere [22]. HUVECs were cultured with M199 supplemented with 10% (v/v) fetal bovine serum (FBS) (Gibco, Thermo Fisher Scientific, Mississauga, ON, Canada), 1% (v/v) Penicillin-Streptomycin (Thermo Fisher Scientific), 2 ng/mL recombinant Human fibroblast growth factor (FGF) (Thermo Fisher Scientific), 0.5 ng/mL recombinant human epidermal growth factor (EGF) (Thermo Fisher Scientific), 1 µg/mL ascorbic acid (Sigma Aldrich, Oakville, ON, Canada), 5 µg/mL insulin (Sigma Aldrich), 1 µg/mL hydrocortisone (Sigma Aldrich), and 90 µg/mL heparin (Sigma Aldrich) within 37^{o}C humidified incubator with 5%CO_2. The samples were sterilized for 10 minutes in ethanol 70%, rinsed three times in PBS 1X solution, and dried under the biological safety hood. The samples of *d*25, *d*75, and *d*150 were placed in 24-well cell culture plate individually. Three samples were involved for each condition (n=3). HUVECs were poured onto each well with the density of 5000 cells/cm^2 for 3 and 5-day incubation periods and 10000 cells/cm^2 for 1-day incubation period. The culture medium was changed every second day allowing fresh supply of nutrients. To measure the metabolic activity of the HUVECs, the medium was removed following the incubation period and 500 µL of fresh medium containing 10% (v/v) resazurin (Sigma Aldrich) was added into each well and incubated for three hours at 37^{o}C with 5%CO_2. Subsequently, 100 µL of medium from each well was transferred into a 96-well plate and absorbance measurement was performed on a spectrophotometer Fluoroskan Ascent (ThermoFisher Scientific) at 450 nm. The proliferation rate of HUVECs was measured by cell counting using hemocytometer following each incubation period by harvesting the cells with 0.5% (v/v) trypsin-EDTA (Thermo Fisher Scientific) for 3-5 minutes at 37^{o}C.

2.4. Fluorescence microscopy

Following the incubation period of HUVECs on the samples, the cells were stained for immunofluorescence. The samples were washed with PBS 1X three times and were then fixed with 3.7% formadehyde in PBS for 20 minutes. The cells were then rinsed with PBS 1X three times and permeabilized with 3% BSA and 0.1% saponin in PBS 1X for 1 minute. DAPI and rhodamine-phalloidine (1/200 in 3% BSA in PBS 1X) were added for an hour of incubation time. The samples were

then washed with 0.05% Tween-20 in PBS 1X three times. The cells were afterward observed under a fluorescence microscope Olympus BX51 (Olympus Corps., Tokyo, Japan).

2.5. Image analysis of cell alignment

For cell orientation study, about 150 cells were analyzed from at least 3 images for each laser patterned surface. The angle between cell orientation and chain-like structure direction (oriented nominally at 0_0) was measured using an image-processing software (ImageJ Version v1.49 Wayne Rasband, National Institutes of Health, USA) as described elsewhere [23]. Briefly, an ellipse was fitted to the cell profile and followed by the measurement between the major ellipse axis and the image y-axis (the direction of chain-like structures), which is defined as alignment angle. The measured angles were then clustered into groups (binned into 10_0 degrees range) representing each alignment angle from -90° to + 90°, with 0° as the reference y-axis of the image (chain-like structure direction).

2.6. Statistical analysis

Results are presented as mean ± standard error unless specified otherwise. Sample inter-group comparison was performed using one-way analysis of variance (one-way ANOVA) and Tukey's post-test. Statistical significance was set at $p<0.05$. Data and statistical analysis were performed using GraphPad Prism version 5.01 for Windows (from GraphPad Software, San Diego, USA).

3.Results

3.1. Laser-structured surface

Figure 2 reports the measured micro-pit width (*w*) and depth (*h*) of the chain-like structure as a function of process parameters. It can be observed that *w* increases with the pulse energy, whereas the increase in scan speed results in a moderate decrease for fixed energy levels (Figure 2A). On the other hand, *h* shows a significant increase at 50 μJ pulse energy (Figure 2B). Below this energy level, *h* decreases to values around 1 μm. With ns-long pulses several mechanism can contribute to the material removal depending on the pulse energy, pulse duration, and beam dimension[24]. For pulsed-laser micromachining, the ablation threshold is considered commonly for describing the material removal behaviour[25]. While the use of this method for ps- and fs-pulsed lasers is adequate, with ns-pulsed lasers the description of a ablation threshold only falls short for describing the differences observed as a function of process parameters[26]. With ns-pulsed lasers, as observed also in this study at lower pulse energy levels, material removal mechanism becomes predominantly based on melt displacement [27]. With an increase in energy levels, melt ejection and vaporisation takes part, providing a more efficient material removal mechanism. Figure 3A shows the micro-pit morphology obtained with E=20 μJ and v=97 mm/s. The morphology is composed of overlapped circles, which are produced by consecutive laser pulses. Each circle exhibits a smaller circle in the centre, which corresponds to the region of effective evaporation. The region between the ablation circle and the border of the wider circle is the product of partial melting and vaporization [28]. The resultant morphology is the so-called chain like structure. This structure has been employed as it fits well with the dimensional requirements of the application. The width of the chain-like structure is adequate to fit the single cell, while the depth is shallow enough to avoid cell entrapment in the pits. Moreover, the treatment is relatively non-invasive for the stent applications, remaining at a limited depth and not-reducing significantly the load-bearing part of the implant. Figure 3 shows the three-dimensional morphology of this structure obtained by AFM. It can be seen that the chain-like structure increases the surface area, as well as provides multiple gripping sites for cells. This condition was chosen for further investigation in surface characterisation as well as the adhesion and proliferation of HUVECs. Average *w* and *h* were measured as 10.1±0.9 μm and 0.64±0.07 μm respectively.

3.2. Surface chemical composition

The survey spectra of XPS showed that metallic elements such as Fe and Cr are present on both electropolished and laser structured surfaces with no significant difference, as showed in Figure 4. Their presence is expected, as they are the alloying elements of SS316L. Moreover, non-metallic elements such as C, N, P, and F were also detected on the surface of the samples. The presence of non-metallic elements suggestively comes from the processing steps of surface preparation since electroforming steps involved different acids and solvents. For comparison purpose, S and P were both found on the electropolished surface of SS316L due to the applied sulphuric and orthophosphoric acids as the electrolyte solution for electropolishing as reported elsewhere [29]. Moreover, both of the surfaces are considered as an oxygen-rich surface. Oxygen binds to chrome forming a passive layer on the surface of SS316L preventing further corrosion. The observed amount of oxygen on both electroformed and laser treated surfaces is comparable. Moreover, carbon surface contamination was also observed on both surfaces. However, this type of contamination is commonly found since isolating the carbon compounds is not a trivial task [30]. One important thing to be emphasized is that the contamination from hydrocarbon compounds was the same for each sample. All the samples were prepared from the same metal sheet, treated with electrolyte similarly, stored within the same conditions, and then measured at the same time. The only difference is the laser treatment applied to specific surface area. Assuming that the laser treatment did not affect the carbon contamination on the surface of SS316L, then the measurement error derived from the contamination was the same for each case.

High resolution XPS scan showed that carbon spectra of both electropolished and laser treated surfaces contain carbon-carbon or carbon-hydrogen peak with binding energy of 284.8 eV, carbon-sulphur or carbon-nitrogen compounds with binding energy of 286.2 eV, and carbon-oxygen bond with binding energy of 288.6 eV [22]. Deconvolution graphs of oxygen species shows the presence of metal oxide (binding energy 529.7 eV), metal hydroxide (binding energy 531 eV), and others (binding energy 532.4 eV) on both surfaces [31]. Moreover, further analysis of Cr and Fe spectra was performed to determine their oxidation states and formed species in the passive film. For both electropolished and laser treated surfaces, oxide compounds in chromium spectra were characterized by the peaks at 577.2 and 578.5 eV[22-23] as seen in Figure 5. The presence of Cr_2O_3 was confirmed by the difference in binding energy of

Cr2p1 and Cr2p3 of 9.79 eV [22]. For iron spectra, the presence of oxide compounds was showed by the presence of 709.4 and 711.8 eV peaks [29-34]. The occurrence of FeOOH was confirmed by the difference of Fe2p1 and Fe2p3 binding energies (13.65 eV) [31]. Referring to the deconvolution graphs of high resolution scans, there is no significant difference between electropolished surface and laser treated surface. The only exception is found on the graph of iron, which showed a higher amount of iron-hydroxide on the laser treated surface (higher fourth component). This is reflected on the O1s peak (higher second component). The third component of the O1s peak, probably part of sulfate, nitrate, phosphate and silicate ions, drops by about half just like the non-metallic elements other than C. The total percentages correspond assuming 2-3 O per other atom: ~11% O1s(3) down to ~6% O1s(3) versus ~6% down to ~2% for the total of S, N, P, Si.

3.3. Metabolic activity, proliferation, and alignment of HUVECs

Metabolic activity—HUVECs showed an increased metabolic activity during the first 24-hour incubation period on *d*25 and *d*75 surfaces compared to the electropolished surface, as described in Figure 6. The metabolic activity remained significantly higher on the *d*25 surface after 3-day incubation period. The metabolic activity of HUVECs remained to be notably higher on *d*25 surface following 5-day incubation period compared to the control and other surfaces. At the same incubation period, the metabolic activity of HUVECs on *d*150 surface was significantly decreased while *d*75 surface was comparable to the control.

Cell proliferation—Following the first day of incubation period, the proliferation rate of HUVECs grown on the *d*25 and *d*75 surfaces tends to increase when compared to the surface of electropolished SS316L (control) as shown in Figure 7. At the end of 3-day incubation period, the proliferation rate of HUVECs on *d*25 surface was significantly higher compared to those on control, *d*75, and *d*150 surfaces. The value was maintained significantly different at the end of 5-day incubation period. Interestingly, the *d*150 surface showed a significantly lower proliferation rate compared to that of the electropolished samples, *d*25, and *d*75 surfaces, which is in accordance with the metabolic activity measurement results.

Cell alignment study—Immunofluorescence staining permits visual observation of their adhesion behaviour on the laser-structured surfaces. Visual observation showed that structured surfaces gave

alignment to the HUVECs parallel to the axis of the chain-like structures, notably for *d*25 surface as seen in Figure 8. Similarly, the result from quantitative measurement of cellular alignment showed that the *d*25 surface gave orientation to the attached HUVECs parallel to the direction of the chain-like structures as seen in Figure 9. Moreover, *d*75 and *d*150 surfaces also gave alignment to the endothelial cells and exhibited alignment angle nearby the axis of the chain-like structure although it is not as prominently observed on *d*25 surface.

4. Discussion

The adhesion of endothelial cells is influenced by both chemical and physical properties of a material[6,7,35]. In the present study, the adhesion of HUVECs was significantly influenced by the presence of chain-like structures generated by laser structuring. The introduction of chain-like structures would presumably change the chemical composition of the SS316L surface. However, XPS survey scan and high resolution spectra showed no significant chemical difference between electropolished and laser structured surfaces except a slightly higher amount of iron-hydroxide and lower amount of impurities on the laser treated surfaces due to the melting process of the SS316L surface following the laser structuring. As oxygen on the surface has been suggested to attract endothelial cells [35], chain-like structures provided more oxygen available since the structures possess an increased surface area compared to that of control surface.

Previous study reported that endothelial adhesion and proliferation were increased on surfaces with an elevated amount of iron, but decreased with elevated amounts of chromium [35]. Similarly, integrated nitrogen on the surface of stainless steel, mainly in the form of CrN and FeN, has been related to endothelial adhesion on the surface [35,36]. However, the current study did not observe significant chemical difference that would affect the behaviour of endothelial cells between laser structured and control surfaces. Therefore, the adhesion of HUVECs in the experiment was mainly influenced by the topography of the chain-like structure.

The topography of the chain-like structure allows mechanical grip within the scanned tracks. The mechanical grip is provided by the presence of micron and sub-micron features on the chain-like structures. This support is minimally found on its counterpart design, grooving. In addition, the

dimensional range of the chain-like structure is suitable for stent applications with the average depth (*h)* of 0.64±0.07 µm. In contrast, the average depth of grooving could be as deep as 5 µm compromising the mechanical properties of newer generations of cardiovascular stents. Thus applying chain-like structure is a promising alternative design to promote endothelialisation for cardiovascular stent applications.

Other than the design, the density of structure apparently played a significant role for the behaviour of endothelial cells. The results are in accordance to the previous reports suggesting that the surface composed of both micro- and nano-topographies might provoke an optimized cellular behaviour in terms of better endothelialisation [37]. It was reported that the optimal endothelial cells adhesion was obtained on the surface of poly(dimethylsiloxane) with periodical grooving of 80 µm. More studies have reported similar size range of grooves (width: 500 nm - 50 µm and depth: 50 nm - 3.5 µm) on the adhesion of endothelial cells [5, 23, 35, 37]. The density of chain-like structure is considerably related to the greater surface area. The laser structured surface constitutes 7%, 13%, and 40% of total *d*150, *d*75, and *d*25 surfaces respectively.

The chain-like structure was shown to give orientation to the endothelial cells because the structure provides a highly ordered pattern. HUVECs are then more likely to be aligned along the direction of the chains. It was shown that *d*25 surface promotes more HUVECs adhesion and alignment starting from 3-day incubation period compared to other surfaces. With this combination of structured and non-structured surface zones, the adhered HUVECs were easily oriented parallel to the direction of structured zone. Aligned endothelial cells have been reported to be resistant against vascular inflammation, whereas dis-aligned endothelial cells at a branch or bifurcation express biological properties that promote atherosclerosis [38]. Therefore, it is suggested that the alignment of endothelial cells provides atheroprotective property [39]. Consequently, surfaces structured with a chain-like structure applied with a distance similar to the cell size can be considered as a potential approach to increase endothelialisation for cardiovascular stent applications.

5. Conclusion

The current work presents a novel surface structure, used for manipulating the cell behaviour on the surface of biomedical implants and consisting of chain-like features produced by partial melting and ablation through pulsed laser irradiation. It is suggested that topographical changes promote the behaviour of HUVECs. The results showed that the structured surfaces favor the adhesion, proliferation, and alignment of HUVECs compared to the control surface. There was no significant difference of chemical composition on the structured surface compared to that of the control suggesting that the behaviours of HUVECs were mainly influenced by the physical structure of the surface. Amongst all the laser-structured surfaces, *d*25 surface was found to significantly facilitate the adhesion, proliferation, and alignment of endothelial cells compared to both *d*75 and *d*150 surfaces. The optimal condition of *d25* suggests that in the absence of any significant chemical changes, spacing of laser structured surfaces close to the cell size is an adequate approach.

6. Acknowledgements

The authors would like to thank Caroline Loy from LBB for the support concerning the cellular tests, Dr. Pascale Chevalier and Dr. Stephane Turgeon from LBB for the surface chemical analysis by XPS, Essowe Mouzou and Yingchao Su for the electropolishing preparation of SS316L. The authors would like to acknowledge the prestigious NSERC Postdoctoral Fellowship awarded to Agung Purnama.

Tables

Table 1. Details of the experimental plan.

Fixed parameters		
Focal position	Δz	50 mm
Pulse repetition rate	PRR	20 kHz
Varied parameters		
Pulse energy	E	30, 40, 50 µJ
Scan speed	v	39, 59, 78, 97 mm/s

Figures

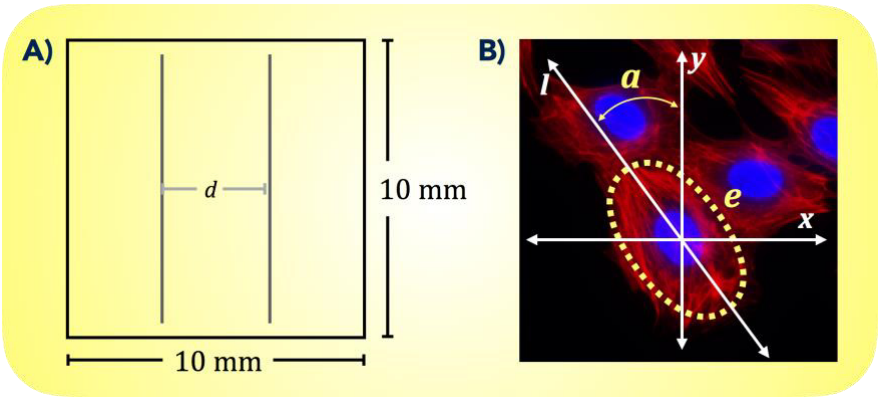

Figure 1. A schematic representation of a SS316L square sample (A). Grey lines within the square represent periodic distance between two adjacent laser structures, represented by *d*. *d* was in the range 25-150 µm; only two machined lines are represented in the drawings, to put in evidence their distance. Measurement of HUVECs orientation on the laser structured surface (B). An ellipse (*e*) was fitted to the cell profile followed by the measurement between the major ellipse axis (*l*) and the direction of the chain-like structures (*y*), which is defined as alignment angle (*a*).

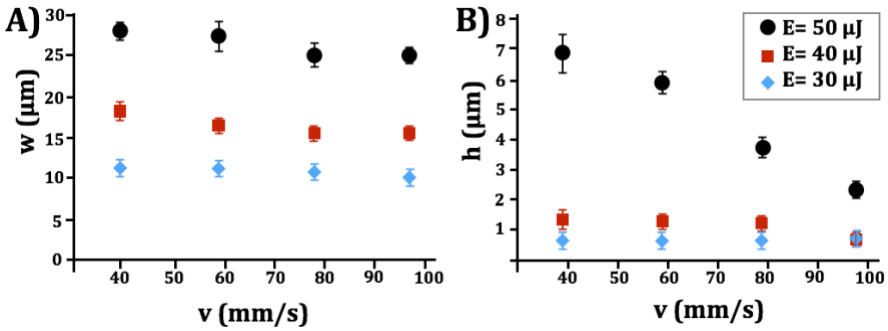

Figure 2. Geometrical characteristics of the laser micromachined micro-pits as a function of process parameters. The width (*w*) of chain-like structure increases with the pulse energy (A), whereas the increase in scan speed results in a moderate decrease for fixed energy levels. Micro-pit depth (*h*) shows a significant increase at 50 µJ pulse energy (B).

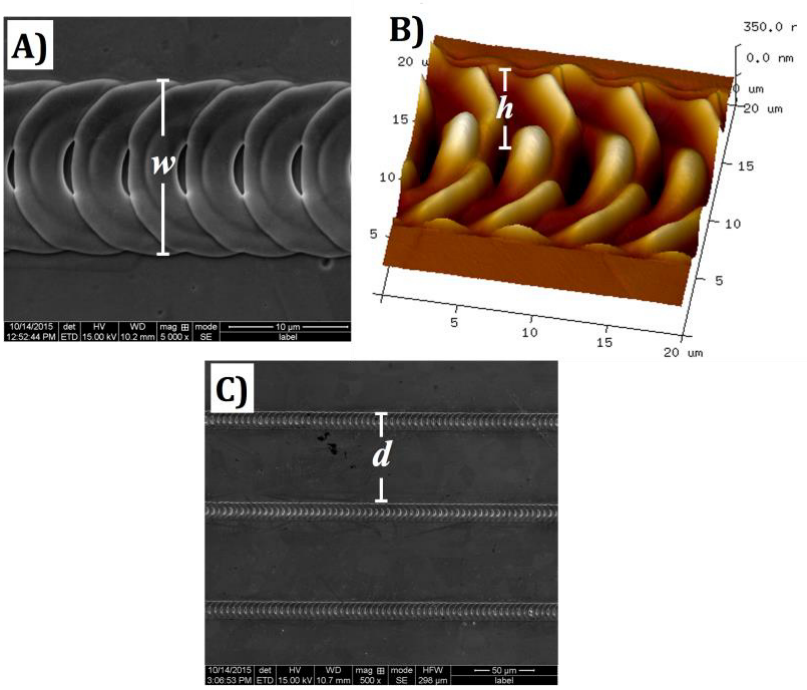

Figure 3. Close-up SEM image of chain-like surface structure following laser treatment, the width of chain-like structure is represented by *w* (A). Topographical characterisation of chain-like structure by AFM, the depth of chain-like structure is represented by *h* (B). SEM image of chain-like *d*75 structure following laser structuring with *d* defined as the periodic distance between two adjacent chains (C).

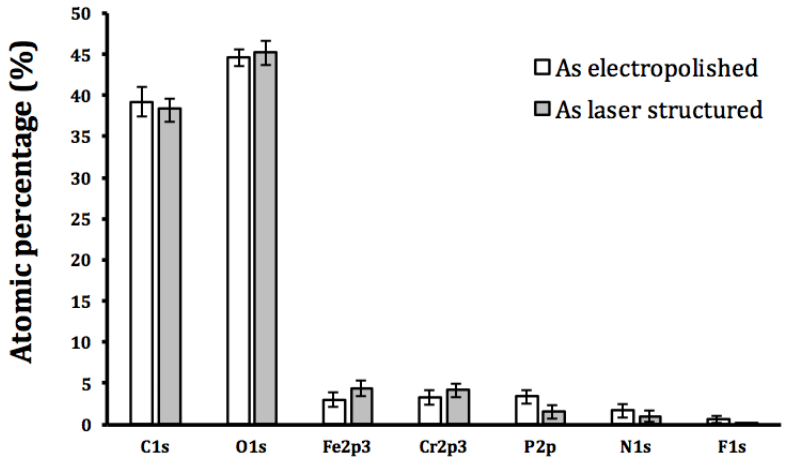

Figure 4. Chemical composition of electropolished and laser structured SS316L surface by XPS analysis.

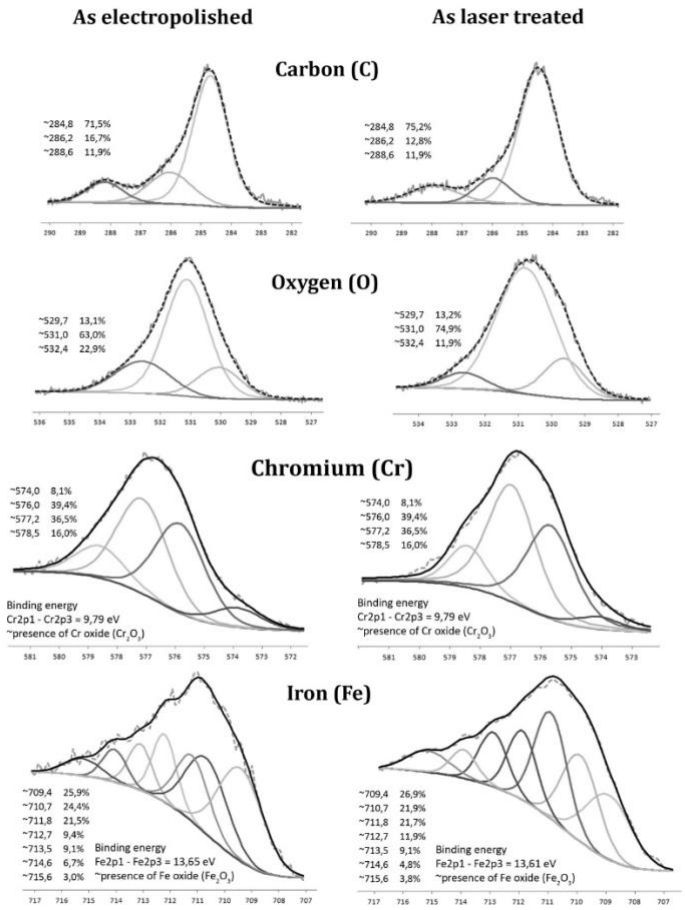

Figure 5. Representative deconvolution graph for carbon, oxygen, chromium, and iron following electropolished and laser structured SS316L surfaces by high resolution XPS analysis.

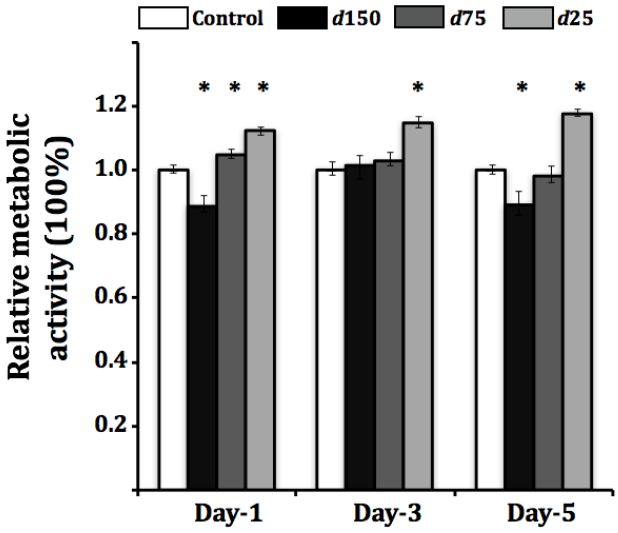

Figure 6. Relative metabolic activity measurement of HUVECs cultured on electropolished and laser structured SS316L surfaces. Relative measurement refers to standardisation of the measured values in which control group was set to 1. $*p<0.05$ with one-way ANOVA followed by Tukey's post test (n=3). Electropolished SS316L was used as a control.

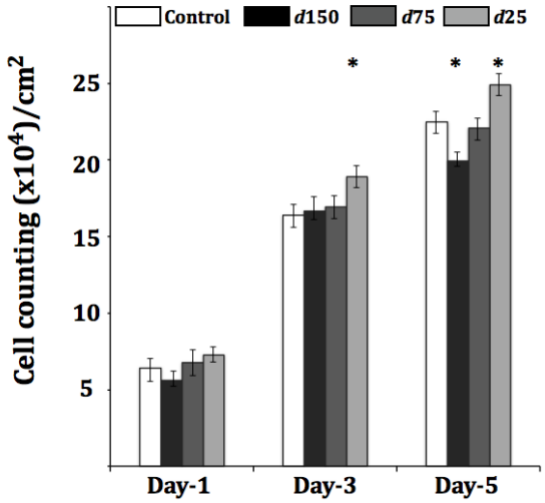

Figure 7. HUVECs proliferation on electropolished and laser structured SS316L surfaces. *$p<0.05$ with one-way ANOVA followed by Tukey's post test (n=3). Electropolished SS316L was used as a control.

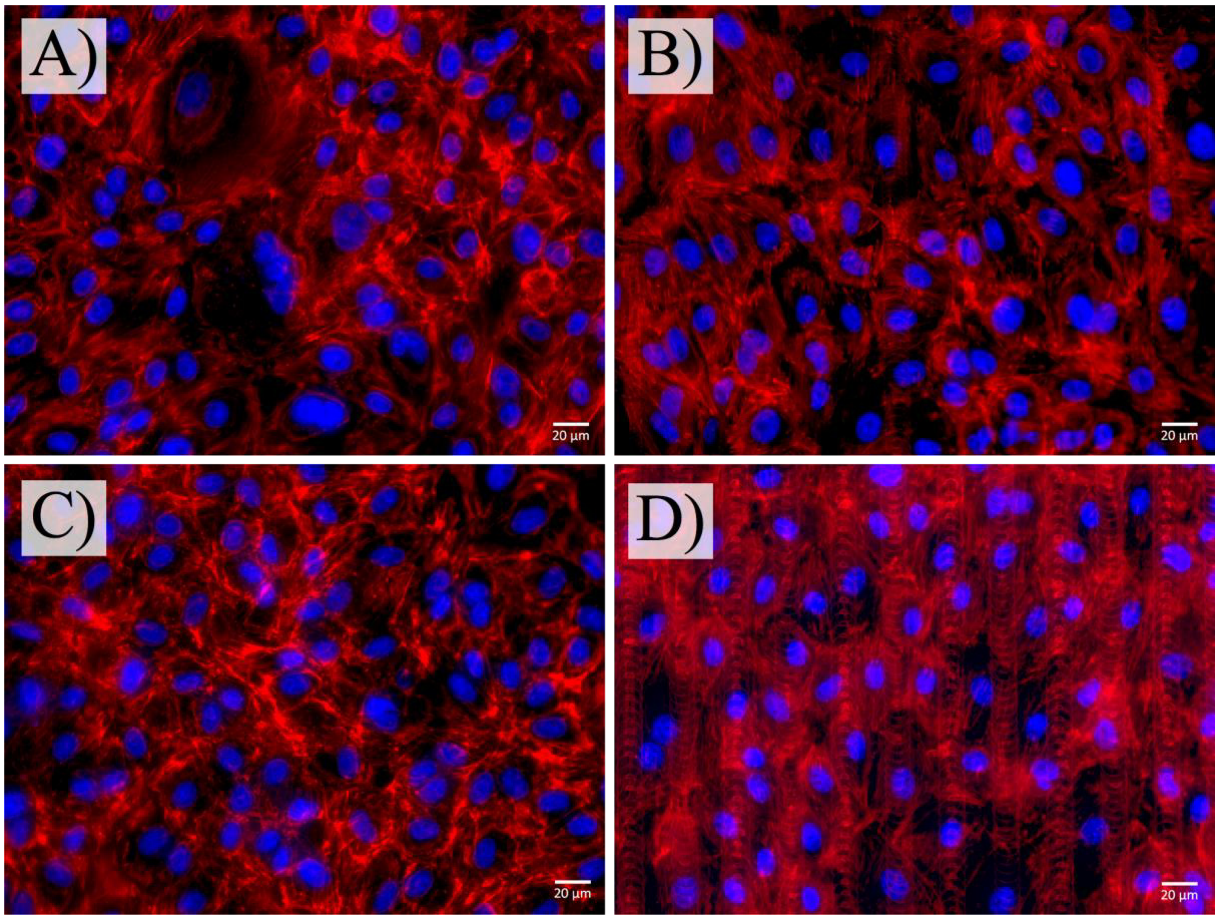

Figure 8. Immunofluorescence staining of HUVECs after 5-day incubation period. Confluent layer of HUVECs layer on electropolished SS316 (A), *d*150 (B), *d*75 (C), and *d*25 (D) surfaces. Cells were stained with DAPI to stain nucleus in blue and rhodamine-phalloidin stain cytoskeleton in red. The scale bar equals to 20 µm in white.

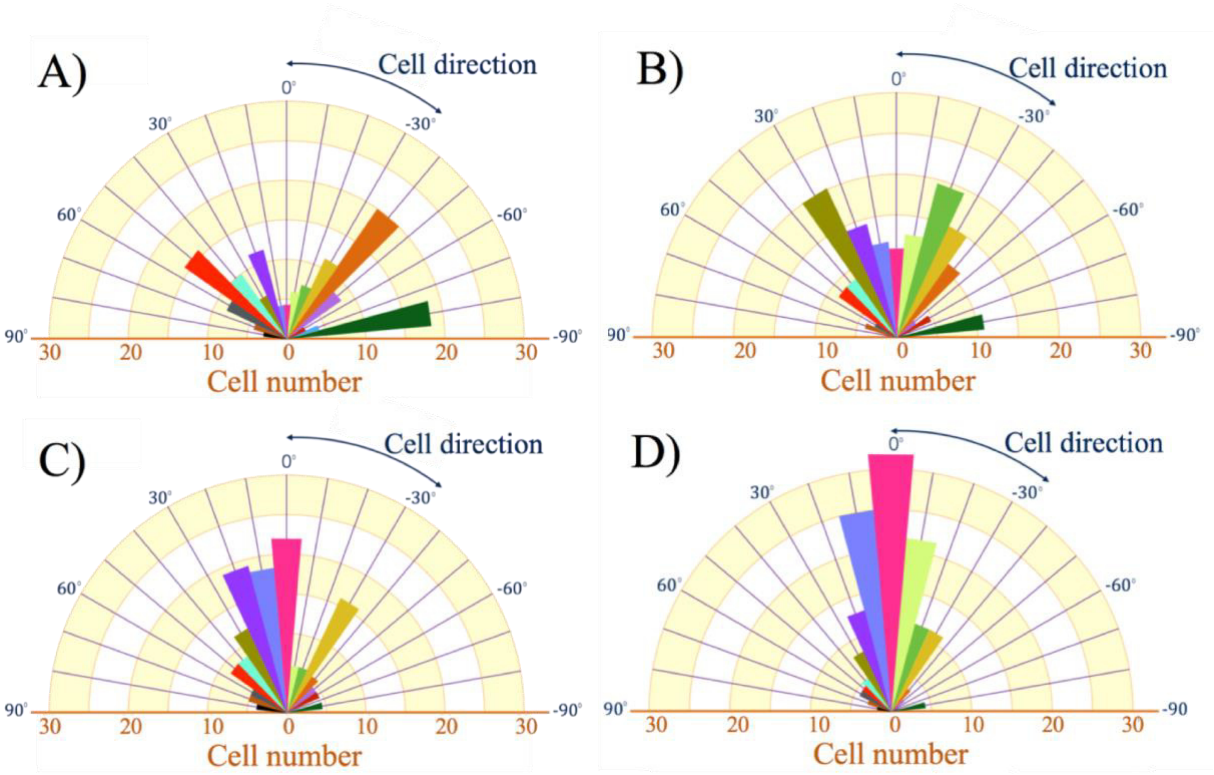

Figure 9. Analysis of the alignment angles of HUVECs. The angles were measured between cell orientation and chain-like structure direction (oriented nominally at 0₀). Distribution of HUVECs orientation on electropolished SS316L surface (A), *d*150 (B), *d*75 (C), and *d*25 (D).

References

[1] G. Li G, P. Yang, W. Qin, M. Maitz, S. Zhou, N. Huang, "The effect of coimmobilizing heparin and fibronectin on titanium on hemocompatibility and endothelialisation", Biomaterials Vol. 32, pp. 4691-4703 (2011)

[2] L. Chen, N. Dong, J. Huang, Z. Zhu, M. Wang, K. Wu, "Effect of vascular nitric oxide pathway on vascular smooth muscle cell proliferation", International Journal of Cardiology Vol. 150, pp. 370-372 (2011)

[3] P.P. Mueller, T. May, A. Perz, H. Hauser, M. Peuster, "Control of smooth muscle cell proliferation by ferrous iron", Biomaterials Vol. 27, pp. 2193-2200 (2006)

[4] A.K. Hassan, S.C. Bergheanu, T. Stijnen, B.L. van der Hoeven, J.D. Snoep, J.W. Plavier, "Late stent malposition risk is higher after drug-eluting stent compared with bare metalstent implantation and associates with late stent thrombosis", European Hearth Journal Vol. 31, pp. 1172-1180 (2010)

[5] J. Lu, M. Rao, N. MacDonald, D. Khang, T. Webster "Improved endothelial cell adhesion and proliferation on patterned titanium surfaces with rationally designed, micrometer to nanometer features", Acta Biomaterialia Vol. 4, pp. 192–201 (2008)

[6] J.C. Palmaz, A. Benson, E.A. Sprague, "Influence of surface topography on endothelialization of intravascular metallic material", J Vasc Interv Radiol Vol. 10, pp. 439–444 (1999)

[7] M. Oberringer, E. Akman, J. Lee, W. Metzger, C.K. Akkan, E. Kacar, A. Demir, H. Abdul-Khaliq, N. Putz, G. Wennemuth, T. Pohlemann, M. Veith, C. Aktas, "Reduced myofibroblast differentiation on femtosecond laser treated 316L stainless steel," Materials Science and Engineering C Vol. 33, pp. 901-908 (2013)

[8] C. De Giorgi, V. Furlan, A.G. Demir, E. Tallarita, G. Candiani, B. Previtali, "Laser micropolishing of AISI 304 stainless steel surfaces for cleanability and bacteria removal capability", Appl. Surf. Sci. 406 (2017).

[9] V. Furlan, M. Biondi, A.G. Demir, G. Pariani, B. Previtali, A. Bianco, "Sub-micrometric surface texturing of AZ31 Mg-alloy through two-beam direct laser interference patterning with a ns-pulsed green fiber laser", Appl. Surf. Sci. Vol. 423, pp. 619-629 (2017).

[10] R. Jagdheesh, M. Diaz and J. L. Ocana, "Bio inspired self-cleaning ultrahydrophobic aluminium surface by laser processing", RSC Adv., Vol. 6, pp. 72933–72941 (2016)

[11] R. Jagdheesh, M. Diaz, S. Marimuthub, J. L. Ocana, "Robust fabrication of m-patterns with tunable and durable wetting properties: hydrophilic to ultrahydrophobic via a vacuum process", J. Mater. Chem. A, Vol. 5, pp. 7125–7136 (2017)

[12] N. Mirhosseini, P.L. Crouse, M.J.J. Schmidth, L. Li, D. Garrod, "Laser surface micro-texturing of Ti–6Al–4V substrates for improved cell integration", Appl. Surf. Sci. Vol. 253, pp. 7738–7743 (2007)

[13] D.G. Waugh, J. Lawrence, E.M. Brown, "Osteoblast cell response to a CO_2 laser modified polymeric material", Opt Lasers Eng Vol. 50, pp. 236–247 (2012)

[14] Qin L, Zeng Q, Wang W, Zhang Y, and Dong G. Response of MC3T3-E1 osteoblast cells to the microenvironment produced on Co-Cr-Mo alloy using laser surface texturing. J Mater Sci 2014;49:2662–2671.

[15] C. Zwahr, D. Günther, T. Brinkmann, N. Gulow, S. Oswald, M. Grosse Holthaus, A.F. Lasagni, "Laser Surface Pattering of Titanium for Improving the Biological Performance of Dental Implants", Adv. Healthc. Mater. 6 (2017)

[16] C. Yiannakou, C. Simitzi, A. Manousaki, C. Fotakis, A. Ranella, E. Stratakis, "Cell patterning via laser micro/nano structured silicon surfaces", Biofabrication. 9 (2017).

[17] V. Dumas, A. Rattner, L. Vico, E. Audouard, J.C. Dumas, P. Naisson, P. Bertrand, "Multiscale grooved titanium processed with femtosecond laser influences mesenchymal stem cell morphology, adhesion, and matrix organization", J. Biomed. Mater. Res. - Part A. Vol. 100 A, pp. 3108–3116 ((2012)

[18] L. Hao, J. Lawrence, K.S. Chian, “Osteoblast cell adhesion on a laser modified zirconia based bioceramic”, J Mater Sci Mater Vol. 16, pp. 719–726 (2005)

[19] T. Kirat, N. Kose, I. Altun, F. Akin, G. Ergun, M.O. Soylu, “What is the most possible cause of the side branch occlusion after bioresorbable everolimus-eluting stent?”, International of Journal Cardiology Vol. 209, pp.348 (2015)

[20] J. Pache, A. Kastrati, J. Mehilli, H. Schuhlen, F. Dotzer, J. Hausleiter, M. Fleckentein, F.J. Neuman, U. Sattelberger, C. Schmitt, M. Muller, J. Dirschinger, A. Schomig, “Angiographic results: strut thickness effect on restenosis outcome (ISAR-STEREO-2) trial”, J Am Coll Cardiol Vol. 41, pp. 1283-1288 (2003)

[21] M. Haidopoulos, S. Turgeon, C. Sarra-Bournet, G. Laroche, D. Mantovani, “Development of an optimized electrochemical process for subsequent coating of 316 stainless steel for stent applications”, J Mater Sci: Mater Med Vol. 17, pp. 647-657 (2006)

[22] V. Montano-Machado, P. Chevallier, D. Mantovani, E. Pauthe, “On the potential for fibronectin/phosphorylcholine coatings on PTFE substrates to jointly modulate endothelial cell adhesion and hemocompatibility properties”, Biomatter Vol. 5, e979679 (2015)

[23] Y. Ding , Z. Yang, C.W. Bi, M. Yang, S.L. Xu, X. Lu, N. Huang, P. Huang, Y. Leng Y, “Directing vascular cell selectivity and hemocompatibility on patterned platforms featuring variable topographic geometry and size”, Appl Mater Interfaces Vol. 6, pp. 12062-12070 (2014)

[24] W. Shulz, U. Eppelt, R. Poprawe, “Review on laser drilling I. Fundamentals, modeling, and simulation”, J. Laser Appl., Vol. 25, No.1, pp. 012006-1-012006-17 (2013)

[25] J.M. Liu, “Simple technique for measurements of pulsed Gaussian-beam spot sizes”, Opt. Lett. Vol. 7, No.5 pp. 196–198 (1982)

[26] A.G. Demir, K. Pangovski, B. Previtali, W. O’Neill, “Laser micromachining of TiN coatings with variable pulse durations and shapes in ns regime”, Surf. Coat. Tech., Vol. 258, pp. 240–248 (2014)

[27] K. Pangovski, P. S. The, D. Lin, S. Alam, D.J. Richardson, W. O’Neill, “Pulse energy packing effects on material transport during laser processing of <111> silicon”, Applied Physics A Vol.124:5, pp.1-9 (2018)

[28] Y. Jee, M. F. Becker, R.M. Walser, “Laser-induced damage on single-crystal metal surfaces”, J. Opt. Soc. Am. B/Vol. 5, No. 3, pp. 648-659 (1988)

[29] T. Hryniewicz, K. Rokosz, R. Rokicki, “Electrochemical and XPS studies of AISI 316L stainless steel after electropolishing in a magnetic field”, Corrosion Science Vol. 50, pp. 2676-2681 (2008)

[30] T. Hryniewicz, K. Rokosz, “Analysis of XPS results of AISI 316L electropolished and magnetoelectropolished at varying conditions,” Surface and Coating Technology Vol. 204, pp. 2583-2592 (2010)

[31] B.V. Crist. Handboook of monochromatic XPS spectra: The elements of native oxides, Volume 3. Wiley, USA.

[32] W. Fredrikson, K. Edstrom, “XPS study of duplex stainless steel as a possible current collector in a Li-ion battery”, Electrochimica Acta Vol. 79, pp. 82-94 (2012)

[33] A.P. Grosvenor, B.A. Kobe, M.C. Biesinger, N.S. McIntyre, “Investigation of multiplet splitting of Fe 2p XPS spectra and bonding in iron compounds”, Surface and Interface Analysis Vol. 36, pp. 1564-1574 (2004)

[34] F. Goutier, S. Valette, E. Laborde, P. Lefort, “304L stainless steel oxidation in carbon dioxide: An XPS study”, Journal of Alloys and Compounds Vol. 509, 3246-3251 (2011)

[35] L. Li, N. Mirhosseini, A. Michael, Z. Liu, T. Wang, “Enhancement of endothelialisation of coronary stents by laser surface engineering”, Lasers in Surgery and Medicine Vol. 45, pp. 608-616 (2013)

[36] S. Britland, H. Morgan, B. Wojiak-Stodart, M. Riehle, A. Curtis, C. Wilkinson, “Synergistic and hierarchical adhesive and topographic guidance of bhk cells”, Exp Cell Res, Vol. 228, pp. 313-325 (1996)

[37] A. Ranjan, T.J. Webster, “Increased endothelial cell adhesion and elongation on micron-patterned nano-rough poly(dimethylsiloxane) films”, Nanotechnology, Vol. 20, pp. 305102 (2009)

[38] J.P. Cooke, “Flow, NO, and atherogenesis”, Proc Natl Acad Sci USA Vol. 100, pp. 768-770 (2003)

[39] N.F. Huang, E.S. Lai, A.J. Ribeiro, S. Pan, B.L. Pruitt, G.G. Fuller, J.P. Cooke, “Spatial patterning of endothelium modulates cell morphology, adhesiveness and transcriptional signature”, Biomaterials Vol. 34, pp. 2928-2937 (2013)